The magnetic structure of Mn_3O_4 Hausmannite between 4.7K and Neel point, 41K

1974 J. Phys. C: Solid State Phys. 7 409

(http://iopscience.iop.org/0022-3719/7/2/019)

J. Phys. C: Solid State Phys., Vol. 7, 1974, Printed in Great Britain.

The magnetic structure of Mn_3O_4 (Hausmannite) between 4·7 K and the Néel point, 41 K

G B Jensen and O V Nielsen
Laboratory for Electrophysics, The Technical University, DK-2800 Lyngby, Denmark

Received 26 June 1973, in final form 13 September 1973

Abstract. A neutron diffraction study has been made on the magnetic structure of single crystalline Mn_3O_4 from liquid helium temperature to the Néel point, 41 K, and the nuclear structure at room temperature has been refined.

Below 33 K the structure may be described in terms of an orthorhombic magnetic unit cell which consists of a chemical BC tetragonal unit cell, doubled in a [010] direction. The magnetic unit cell contains 8 chemical formula units. The moments of the 8 Mn^{2+} ions on tetrahedral sites are ferromagnetically aligned parallel to a [010] direction, whereas the moments of the 16 octahedral site Mn^{3+} ions form a more complicated ordered configuration with two sets of 8 symmetry-related single ion moment directions; one of these sets is responsible for the magnetic cell doubling. The resultant moment for the Mn^{3+} ions is antiparallel to the Mn^{2+} moments, which at helium temperature gives rise to a total moment of 15·1 Bohr magnetons per magnetic unit cell. The proposed structure deviates somewhat from a structure previously reported on the basis of powder data.

A phase transition has been observed at 33 K; from 33–39 K it is found that the moments, which at lower temperature give rise to the magnetic cell doubling, form a spiral structure with a [010] directed propagation vector. The pitch length is non compatible with the chemical lattice constant.

From 39 K to the Néel point 41 K, the magnetic unit cell coincides with the BC chemical unit cell.

A special feature in the magnetic structure of Mn_3O_4 below 33 K allows a fairly accurate experimental determination of the atomic form factor curve for Mn^{3+} ions.

1. Introduction

Mn_3O_4 has a tetragonally distorted spinel structure for temperatures below 1443 K. The high temperature phase is cubic and isomorphous with spinel. At room temperature, the lattice constants for the body-centred tetragonal cell are $a = b = 5{\cdot}71$ Å and $c = 9{\cdot}35$ Å. The more natural choice of a face centered tetragonal unit cell with $a_1 = a_2 = 5{\cdot}71\sqrt{2}$ Å and $c = 9{\cdot}35$ Å will not be used here, although it is better suited to show the relation to the FC cubic cell of the spinel structure.

The space group is $I4_1/amd$ (No. 141) with manganese in positions fixed by symmetry (4(a) and 8(d)) and oxygen in 16(h). The nuclear structure thus contains only 2 parameters (α, β) referring to 16(h), a position from this set being (0, α, β). The values found by x-ray methods are $\alpha = 0{\cdot}216$ and $\beta = 0{\cdot}384$ (Satomi 1961). The ionic structure is $Mn^{2+}[Mn_2^{3+}]O_4$ (Goodenough and Loeb 1955, Satomi 1961), ie Mn^{2+} ions occupy sites 4(a) (tetrahedral or A sites) and Mn^{3+} are in sites 8(d) (octahedral or B sites).

The magnetic properties can be reviewed shortly as follows (Dwight and Menyuk 1960, Moruzzi 1961, Nielsen 1971). Below 41 K the magnetic response indicates a magnetic ordering with a resultant magnetization $\boldsymbol{M}$ in the direction of one of the main crystallographic axes ($\boldsymbol{a}$ or $\boldsymbol{b}$) in the basal plane. By convention, the direction of $\boldsymbol{M}$ is chosen as the [010] (ie $\boldsymbol{b}$) direction. [001] is the hard direction of magnetization. Above 41 K the response is paramagnetic, and the [001] anisotropy persists up to 100 K, above which temperature the susceptibility is isotropic.

The magnetic unit cell at 4·2 K has previously been determined by neutron diffraction on powdered samples (Kasper 1959, Boucher *et al* 1971), and a magnetic structure, which roughly agrees with our results, has been determined by Boucher *et al* (1971). The unit cell is orthorhombic and contains two chemical unit cells, a cell doubling occurring in the direction of $\boldsymbol{M}$, or, by the convention mentioned above, in the [010] direction.

All indices in the following refer, unless otherwise stated, to this magnetic unit cell with lattice constants a, $2a$, c. The position vector for the jth atom is denoted by $\boldsymbol{r}_j = x_j\boldsymbol{a} + y_j\boldsymbol{b} + z_j\boldsymbol{c}$ ($b = 2a$), and the scattering vector by $\boldsymbol{H} = 2\pi(h\boldsymbol{a}^* + k\boldsymbol{b}^* + l\boldsymbol{c}^*)$. The conventional symbols for Bragg angle (θ), scattering amplitude (F) and integrated intensity (I) are used below.

2. Experimental

The single crystal used in our experiments was grown from a Borax flux (Nielsen 1969). The crystal (mass 22·7 mg) has the shape of a 0·6 mm thick triangular flake, where the main crystal face (the plane of the triangle) is parallel to a crystallographic 5·71 Å axis. Thus one of the two easy directions lies (fortunately) in the crystal plane, making possible a single domain configuration with negligible demagnetization. Following the conventions mentioned above, this direction is chosen as the $\boldsymbol{b}$ or [010] direction. The main crystal face has indices (1, 0, 1). In order to induce the desired single domain configuration, a magnetic field $\boldsymbol{H}_0$($H_0 \simeq 1800$ gauss) was applied in the [010] direction during the cooling process to liquid helium temperature.

All diffraction experiments were performed in zero applied field and with neutron wavelength 1·150 Å (unpolarized). Initial scans at 4 K showed presence of fairly strong

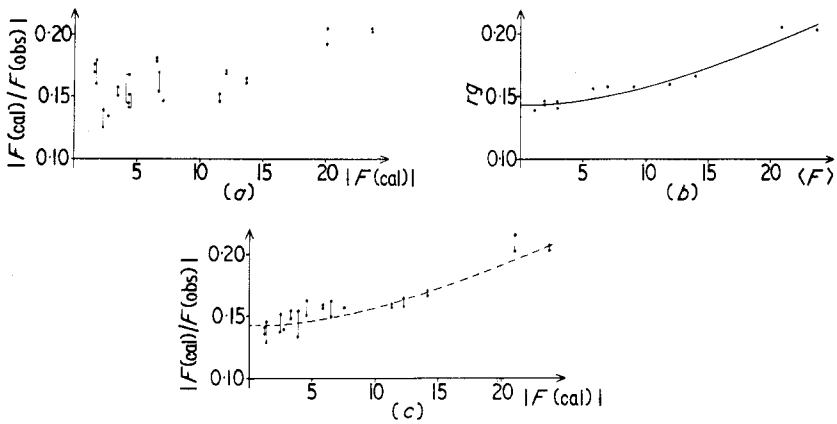

Figure 1. Ratios between calculated and observed structure amplitudes. (*a*) Ratios for oxygen parameter $\alpha = 0{\cdot}216$, $\beta = 0{\cdot}384$ (Satomi 1961). (*b*) Products rg were r is the extinction free scale factor and g the extinction correction. (*c*) Ratios for refined oxygen parameters $\alpha = 0{\cdot}2208$, $\beta = 0{\cdot}3834$. The broken line represents rg.

coherent peaks with indices $(1, \frac{1}{2}, 0)$ and $(\bar{1}, \frac{1}{2}, 0)$ referred to the chemical cell, showing as expected that the cell doubling direction, ie the $\boldsymbol{b}$ axis of the magnetic cell, is in the direction of the magnetization $\boldsymbol{M}$. Furthermore, the absence of a coherent $(\frac{1}{2}, 1, 0)$ peak (chemical indices) showed the crystal to be in single domain configuration. This conclusion is confirmed by one particular experiment, where the crystal was cooled in zero field to 4 K. It was here found that $I(1, \frac{1}{2}, 0) = I(\frac{1}{2}, 1, 0) = \frac{1}{2}I_1(1, \frac{1}{2}, 0)$, where all indices are based on the chemical cell, and the last intensity refers to the single domain configuration.

The intensities for the single domain configuration were measured at 4 K for 74 reflections belonging to 3 different reciprocal lattice planes through the origin (see table 2). Several of these intensities were followed as a function of temperature, and more complete scans were made at 29 K, 34 K and 300 K. In the latter case, where all coherent peaks are purely nuclear, the scan covered only the 30 reflections permitted by the space group, and in addition the non-allowed $(\bar{1}20)$ reflection, which is present due to second order contamination ($\lambda = 0{\cdot}575$ Å) in the primary beam. In all tables below, a correction for this effect (of relative magnitude $1{\cdot}7 \times 10^{-3}$) has been made where significant. Absorption corrections have been omitted because of the small value $\mu = 0{\cdot}43\ \text{cm}^{-1}$ for the absorption coefficient.

3. Refinement of the nuclear structure

The 300 K data were used to find the scale factor r converting the observed structure amplitudes F(obs) to the scale of the calculated values F(cal). Because of the difficulties mentioned below, the value of r was found by a special method to be described in some detail. First, it is noted that r is for the following reason an important parameter in the magnetic structure determination. In Mn_3O_4, the moments largely cancel when summed, as seen from the low net magnetization $M = 15{\cdot}1\ \mu_B$ for the 24 Mn ions in the unit cell. In determining the individual moment lengths, the value of M is consequently relatively unimportant as compared with the value of the scale factor. In fact, r enters to a first approximation as a common factor to all moment lengths.

A comparison of F(obs) and F(cal) for the 300 K data is shown in figure 1*a*. Here, F(cal) is obtained from the following expression using the oxygen parameters and the Debye–Waller factor ($B = 0{\cdot}18$ Å^2) as determined by x-ray methods (Satomi 1961):

$$F(\text{cal}) = \sum_{\mathbf{K}} b_{\mathbf{K}} \exp(-\mathrm{i}\,\boldsymbol{H}\,.\,\boldsymbol{r}_{\mathbf{K}}) \exp(-B \sin^2\theta/\lambda^2). \tag{1}$$

In this as well as later applications of (1), the summation is extended over the magnetic instead of the chemical unit cell. The scattering lengths are b(oxygen) = 0·5803 and b(manganese) = −0·377 in units of 10^{-12} cm. F(obs) is defined as $(I(\text{obs})/L)^{1/2}$, where I(obs) is the observed integrated intensity and $L = 1/\cos\theta$ is the Lorentz factor for the type of scan used in all measurements. Each scan was performed in zero-layer geometry as a step scan with equidistant steps in reciprocal space along a line perpendicular to the reciprocal lattice vector for the reflection. The effect of experimental errors in figure 1*a* can be estimated from the vertical lines connecting points for symmmetry related reflections as eg $(0\bar{4}2)$ and $(\bar{2}02)$.

In figure 1*a*, the upward trend for increasing F(cal) shows the presence of a considerable extinction for the strong reflections. Furthermore, the spread of the points for low values of F(cal) indicates that the oxygen parameters α and β as determined by x-ray methods need refinement.

Because of the extinction, this refinement can not be performed by simply minimizing

$\Sigma(rF(\text{obs}) - |F(\text{cal}; \alpha, \beta)|)^2$ with respect to r, α and β. Instead, $F(\text{obs})$ must be replaced by $gF(\text{obs})$, where g is an extinction correction. It can be assumed *a priori* that g is an increasing function of F with the property $g \to 1$ for $F \to 0$, but g is otherwise unknown. The difficulty thus present in the refinement procedure was circumvented in the following way: For each of the 30 reflections, the coefficients A and B were calculated for the expansion

$$|F(\text{cal}; \alpha, \beta)| = |F(\text{cal}; \alpha_0, \beta_0)| + A(\alpha - \alpha_0) + B(\beta - \beta_0),$$

where α_0, β_0 are Satomi's values. For a set of 3 reflections it is now possible to form a linear combination

$$S(\text{cal}) = k_1|F_1| + k_2|F_2| + k_3|F_3|$$

so that $S(\text{cal})$ is independent of α and β (in special cases two or even one F-value is sufficient). In the same linear combination of the corresponding values $F(\text{obs})$ is called $S(\text{obs})$, the ratio $S(\text{cal})/S(\text{obs})$ gives a value for the product rg unaffected by even relatively large inaccuracies in α and β. Ideally, such invariant linear combinations should contain 3 nearly equal F values and k's of equal sign in order to improve accuracy. In all, 12 satisfactory sets were found. In figure 1*b*, the resulting values of rg are plotted versus the average F values of each set. The curve shows the effect of extinction and leads to the value $r = 0{\cdot}143 \pm 0{\cdot}002$ for the scale factor. Using this value and a Debye–Waller correction with $B = 0{\cdot}18$ Å^2, the oxygen parameters were finally found from a least squares analysis on the 13 weakest reflections, where extinction is seen to be negligible. The reliability factor, defined as $R = \Sigma\{|r|F(\text{obs})| - |F(\text{cal})||/r|F(\text{obs})|\}$ has the value 5·8 % for these reflections. Figure 1*c* shows a plot similar to figure 1*a* except that the new parameters α, β are used. The dotted line is the extinction curve (figure 1*b*). The improvement over figure 1*a* reflects the favourable change in scattering power ratio (oxygen to manganese) in changing from x-ray to neutron diffraction.

In table 1, α and β as found here are compared with values previously published.

Table 1. Oxygen parameters

	Satomi	Boucher *et al*	Present Work
α	0·216	0·227	$0{\cdot}2208 \pm 7$
β	0·384	0·383	$0{\cdot}3834 \pm 5$

A list of $F(\text{obs})$ (properly scaled) and $F(\text{cal})$ based on $\alpha = 0{\cdot}2208$ and $\beta = 0{\cdot}3834$ is given in table 2, columns 2 and 3. It is seen that the effect of extinction at room temperature is very marked for the 4 strongest reflections, ie $(04\bar{2})$, $(\bar{2}02)$, $(\bar{2}8\bar{2})$ and $(\bar{4}42)$, where the observed intensities are only about 50 % of those calculated.

As no phase transitions have been reported for Mn_3O_4 in the temperature range 300 K to 41 K (the Néel point), it was expected that the neutron diffraction intensities should stay constant in this range, apart from slight variations due to change in the Debye–Waller factor. However, the intensities of the 4 strongest reflections, when measured at 45 K, were about 33 % larger than the corresponding intensities at 300 K (for $(\bar{2}02)$ the increase was only 20 %). The reflection $(04\bar{2})$ was measured also at 95 K, where the intensity was still 33 % above that at 300 K. On the other hand, each of the weak reflections $(\bar{1}\bar{2}2)$ and (040) had the same intensity at 45 K as at 300 K. (No other reflections were measured at temperatures between 45 K and 300 K.) The remaining part of this section deals with experiments from which we conclude that the intensity changes mentioned are due to extinction effects.

In order to check for a possible change in the nuclear structure, an x-ray exposure was made from a small single crystal in a Weissenberg goniometer at 300 K and at approximately 150 K. Only the zero-layer line in rotation around the chemical [111] direction was recorded at both temperatures. The two exposures showed the same relative intensities and were in fact identical except for a visible change in the lattice constants. Thus, no structural change occurs between 150 K and 300 K, a fact of importance for the conclusion drawn below.

After all other measurements were completed, the intensity changes mentioned above were investigated in more detail by neutron diffraction. For these measurements, the crystal mounting is referred to as the second mounting, because it differed from the one originally used (ie the first mounting). The change in mounting was incidental and not at the time thought to be of any consequence. For the second mounting, the intensity of the $(04\bar{2})$ reflection was found to increase practically linearly with decreasing temperature in the range 300 K to 95 K, until at 95 K the intensity was about 20% above the value at 300 K. The same behaviour was found for the $(\bar{2}8\bar{2})$ reflection. This shows firstly, that the previously found change of 33% over the same temperature range (and with the first mounting) was not reproducible, and secondly, that the neutron diffraction intensities for these strong reflections thus showed a considerable change between the two temperatures, where no similar effect was seen using x rays (and a different sample).

Based on this, it was concluded that the intensity changes mentioned were due to a change in the primary extinction, caused by a deformation of the thin plate used as neutron diffraction sample. This explains the dependence of the intensity change on crystal mounting, as the stresses responsible for the deformation will depend on the quantity and distribution of glue used (the two mountings differed considerably in this respect). It also explains the unchanged intensities for the extinction-free reflections $(\bar{1}\bar{2}2)$ and (040).

Thus, our data do not indicate any structural change between 300 K and 45 K. Furthermore, at the end of §4 it will appear that a satisfactory fit is obtained at 4 K using the nuclear structure as found at 300 K. Even considering the complication of magnetic contributions, it can be safely concluded that the nuclear structure is practically unchanged in the range 300 K to 4 K.

For all data used in the refinements, the crystal mounting was unchanged (the first mounting) and the intensities at a given temperature completely reproducible. The fact that extinction is much smaller at low temperature than at 300 K is of great help in the magnetic structure determination.

4. The magnetic structure at 4·7 K

The magnetic structure amplitude $\boldsymbol{F}$ and intensity I are, on the same scale as used in (1), given by

$$\boldsymbol{F} = \tfrac{1}{2} r_0 \gamma \{[\sum_j f_j \boldsymbol{\mu}_j \exp(-i\boldsymbol{H} \cdot \boldsymbol{r}_j)] \times \boldsymbol{H}\} \times \boldsymbol{H}/H^2 \qquad (2)$$

$$I = \boldsymbol{F} \cdot \boldsymbol{F}^* L \qquad \text{with } L = 1/\cos\theta.$$

The sum in (2) is over all Mn ions in the magnetic cell. The ion at $\boldsymbol{r}_j$ has the form factor f_j and a magnetic moment $\boldsymbol{\mu}_j$ in units of the Bohr magneton μ_B. Furthermore, $r_0 = e^2/4\pi\epsilon_0 mc^2 = 2{\cdot}818 \times 10^{-13}$ cm and $\gamma = 1{\cdot}913$. Figure 3 shows the numbering chosen for the Mn ions. As seen, all odd-numbered ions lie in one chemical cell, all

Table 2. Comparison of observed and calculated structure factors and magnetic Q vectors for the Mn_3O_4 magnetic unit cell.

(*a*) Zero intensity reflections (observed and calculated). k odd: 030, 210, $\bar{2}10$, 050, 230, $\bar{2}30$, 410, $4\bar{1}0$, and (from powder pattern) 010, 011, $01\bar{1}$, 012, $01\bar{2}$. k even: 020, $\bar{1}00$, $\bar{2}01$, $\bar{2}20$, 220, $\bar{1}40$, 140, $22\bar{2}$, $\bar{2}4\bar{1}$, 060, $\bar{3}00$, $24\bar{3}$, $2\bar{6}2$.

(*b*) Nonzero reflections, k odd (first part) and k even (second part).

	Nuclear contribution (300 K)		Magnetic contributions (4·7 K)				Total (4·7 K)	
hkl	$\lvert F_{exp}\rvert$ (10^{-12} cm)	$\lvert F_{cal}\rvert$ (10^{-12} cm)	$\lvert F_{exp}\rvert$ (10^{-12} cm)	$\lvert F_{cal}\rvert$ (10^{-12} cm)	$\lvert Q_{exp}\rvert$† (μ_B)	$\lvert Q_{cal}\rvert$† (μ_B)	$\lvert F_{exp}\rvert$ (10^{-12} cm)	$\lvert F_{cal}\rvert$ (10^{-12} cm)
$\bar{1}10$	0·0	0·0	4·02	4·22	16·6	17·4	4·02	4·22
110	0·0	0·0	4·36	4·22	17·9	17·4	4·36	4·22
$11\bar{1}$	0·0	0·0	3·49	3·58	14·9	15·2	3·49	3·58
$\bar{1}30$	0·0	0·0	3·74	3·59	18·1	17·4	3·74	3·59
130	0·0	0·0	3·96	3·59	19·1	17·4	3·96	3·59
$\bar{1}3\bar{1}$	0·0	0·0	3·00	3·31	14·9	16·5	3·00	3·31
$13\bar{2}$	0·0	0·0	2·46	2·67	13·2	14·4	2·46	2·67
$\bar{1}5\bar{2}$	0·0	0·0	2·13	2·26	14·9	15·8	2·13	2·26
$\bar{3}10$	0·0	0·0	2·58	2·41	18·6	17·4	2·58	2·41
310	0·0	0·0	2·65	2·41	19·1	17·4	2·65	2·41
$\bar{3}11$	0·0	0·0	2·30	2·31	17·0	17·0	2·30	2·31
$15\bar{3}$	0·0	0·0	1·78	1·84	13·9	14·4	1·78	1·84
$31\bar{2}$	0·0	0·0	2·08	2·05	16·3	16·1	2·08	2·05
$\bar{3}30$	0·0	0·0	2·10	2·14	17·1	17·4	2·10	2·14
$\bar{3}\bar{3}0$	0·0	0·0	2·17	2·14	17·6	17·4	2·17	2·14
$33\bar{3}$	0·0	0·0	1·52	1·52	15·2	15·2	1·52	1·52
$35\bar{1}$	0·0	0·0	1·41	1·60	15·2	17·2	1·41	1·60
$\bar{1}7\bar{3}$	0·0	0·0	1·33	1·35	15·3	15·5	1·33	1·35
$0\bar{2}1$	1·28	1·27	9·25	9·58	39·0	40·4	9·34	9.66
$\bar{1}01$	1·34	1·27	8·44	8·40	35·6	35·4	8·54	8·49
$\bar{1}20$	0·0	0·0	6·28	6·12	28·2	27·4	6·28	6·12
120	0·0	0·0	6·21	6·12	27·8	27·4	6·21	6·12
$\bar{1}\bar{2}2$	2·82	2·73	5·21	5·25	26·5	26·7	5·93	5·92
040	2·58	2·46	1·59	0·0	6·8	0·0	3·04	2·46
$\bar{2}00$	2·33	2·46	5·81	5·88	30·7	31·0	6·27	6·37
$1\bar{4}1$	6·19	6·47	2·20	1·04	12·7	6·1	6·61	6·55
$2\bar{2}\bar{1}$	5·66	6·47	4·39	5·41	25·7	31·6	7·19	8·43
$04\bar{2}$‡	16·74	23·86	9·20	1·81	54·3	10·7	19·22	23·93
$\bar{2}02$‡	16·49	23·86	7·00	3·47	41·3	20·5	18·03	24·11
$\bar{2}40$	12·11	14·08	7·13	5·35	50·2	37·8	14·17	15·07
240	11·84	14·08	8·12	5·35	57·1	37·8	14·46	15·07
$14\bar{3}$	3·59	3·90	3·55	3·48	25·6	25·2	5·08	5·23
$\bar{2}\bar{2}3$	4·18	3·90	6·13	5·92	44·2	42·7	7·45	7·09
$\bar{3}20$	0·0	0·0	3·47	3·56	28·0	28·7	3·47	3·56
320	0·0	0·0	3·61	3·56	29·1	28·7	3·61	3·56
$1\bar{6}2$	3·26	3·38	4·68	4·46	41·8	39·8	5·73	5·59
$\bar{3}22$	3·12	3·38	4·47	4·44	39·9	39·6	5·48	5·57
$0\bar{6}3$	10·26	11·35	3·76	1·96	35·6	18·6	11·09	11·52
$\bar{3}03$	10·12	11·35	3·62	1·06	34·6	10·1	10·92	11·40
$\bar{2}6\bar{1}$	0·0	0·02	2·50	2·69	25·5	27·5	2·50	2·69
$\bar{3}41$	0·0	0·02	1·40	0·80	14·3	8·1	1·40	0·80
$24\bar{4}$	6·83	7·51	2·56	0·73	27·4	7·8	7·42	7·55
$1\bar{6}4$	1·47	1·34	2·06	1·98	25·4	24·6	2·55	2·40
$32\bar{4}$	1·31	1·34	1·90	2·07	23·6	25·6	2·33	2·47
$\bar{3}60$	0·0	0·0	2·08	2·14	29·6	30·5	2·08	2·14

Table 2.—*continued*

$\bar{1}8\bar{3}$	4·02	4·57	1·53	0·23	25·9	3·9	4·41	4·58
$\bar{4}23$	4·32	4·57	2·64	1·89	44·5	32·0	5·17	4·95
$\bar{2}8\bar{2}$ ‡	13·91	21·03	7·25	0·63	132·0	11·4	16·05	21·04
$\bar{4}42$‡	14·96	21·03	7·69	1·12	139·9	20·3	17·23	21·06
$0\bar{8}4$	11·18	12·35	4·30	1·45	80·5	27·2	12·30	12·43
$40\bar{4}$	10·75	12·35	3·06	2·78	57·4	52·0	11·50	12·65
$26\bar{5}$	5·29	5·86	2·72	2·28	52·0	43·6	6·09	6·29
$34\bar{5}$	5·23	5·86	2·06	1·59	39·6	30·4	5·78	6·07

† When Q is composed of contributions both from Mn^{2+} and Mn^{3+} ions (k even), the mean value of their form factors is used in the conversion from observed and calculated intensities to Q-vectors.

‡ Reflections which have been omitted in the calculation of the overall R-value.

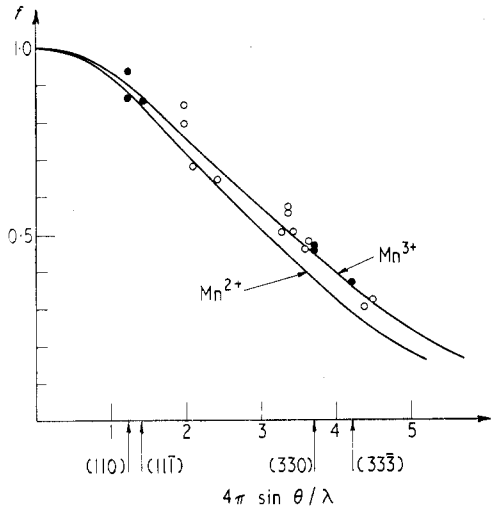

Figure 2. Atomic form factor curve for Mn^{3+}. The curve for Mn^{2+} is taken from Hastings *et al* (1959). ●'Structure independent' experimental points (see text); ○Further experimental points for the structure described in the text.

even-numbered in the adjacent chemical cell which, together with the first, constitutes the magnetic cell.

It is useful in calculating $\boldsymbol{F}$ from (2) to distinguish between k even and k odd. The corresponding values $\boldsymbol{F}_{k-\text{even}}$ and $\boldsymbol{F}_{k-\text{odd}}$ are given by the following, where Σ'_j indicates a sum over odd j ($j = 1, 3 \ldots 23$):

$$\boldsymbol{F}_{k-\text{even}} = \tfrac{1}{2}r_0\gamma\{[\textstyle\sum_j{}' f_j \boldsymbol{p}_j \exp(-i\boldsymbol{H}\cdot\boldsymbol{r}_j)] \times \boldsymbol{H}\} \times \boldsymbol{H}/H^2 \qquad (3a)$$

$$\boldsymbol{F}_{k-\text{odd}} = \tfrac{1}{2}r_0\gamma\{[\textstyle\sum_j{}' f_j \boldsymbol{d}_j \exp(-i\boldsymbol{H}\cdot\boldsymbol{r}_j)] \times \boldsymbol{H}\} \times \boldsymbol{H}/H^2 \qquad (3b)$$

where

$$\boldsymbol{p}_j = \boldsymbol{\mu}_j + \boldsymbol{\mu}_{j+1} \qquad j \text{ odd only}$$

$$\boldsymbol{d}_j = \boldsymbol{\mu}_j - \boldsymbol{\mu}_{j+1} \qquad j \text{ odd only.}$$

Hence, the structure determination separates in two parts: determination of the 'moment sum' system from even-k reflections, and the 'moment difference' system from

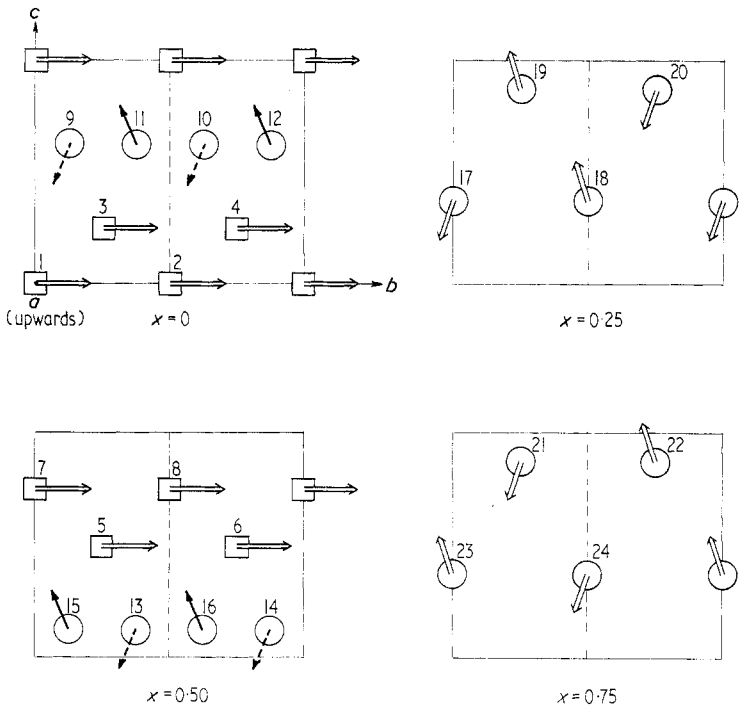

Figure 3. Magnetic structure for Mn_3O_4 at 4·7 K. Magnetic moment magnitudes and direction cosines are given in table 3. □tetrahedral site: ○octahedral site: ⇒moment in the plane; →moment directed upwards;⇢ moment directed downwards.

odd-k reflections. In the initial steps of this program all f_j can be assumed equal for a given length of $\boldsymbol{H}$. The complex vectors $\boldsymbol{P}$, $\boldsymbol{D}$ and $\boldsymbol{Q}$ defined below are then convenient:

$$\boldsymbol{P}(hkl) = \sum_j{}' \boldsymbol{p}_j \exp(-\mathrm{i}\boldsymbol{H} \cdot \boldsymbol{r}_j) \text{ and } \boldsymbol{D}(hkl) = \sum_j{}' \boldsymbol{d}_j \exp(-\mathrm{i}\boldsymbol{H} \cdot \boldsymbol{r}_j) \tag{4a}$$

$$\boldsymbol{Q}(hkl) = ((\sum_j \boldsymbol{\mu}_j \exp(-\mathrm{i}\boldsymbol{H} \cdot \boldsymbol{r}_j)) \times \boldsymbol{H}) \times \boldsymbol{H}/H^2. \tag{4b}$$

The special positions occupied by Mn have coordinates which, referred to the magnetic cell, are integral multiples of $\frac{1}{8}$. This simplifies the handling of equation (4) considerably.

4.1. Zero-intensity reflections

4.1.1. k odd. These reflections are listed in table 2. It is found from (4) that

$$\boldsymbol{D}(010) = \boldsymbol{D}(410), \boldsymbol{D}(210) = \boldsymbol{D}(\bar{2}10) \text{ and } \boldsymbol{D}(230) = \boldsymbol{D}(\bar{2}30). \tag{5}$$

Because the two scattering vectors entering in each equation are non-parallel, it is concluded from the observed zero intensities that all complex vectors in (5) are zero. On reduction, this leads to

$$\boldsymbol{d}_1 + \boldsymbol{d}_7 = \boldsymbol{d}_3 + \boldsymbol{d}_5 = \boldsymbol{d}_9 + \boldsymbol{d}_{15} = \boldsymbol{d}_{11} + \boldsymbol{d}_{13} = \boldsymbol{d}_{17} + \boldsymbol{d}_{23} = \boldsymbol{d}_{19} + \boldsymbol{d}_{21} = \boldsymbol{0}. \tag{6}$$

From a powder pattern, we have further measured the intensities $I(011) = I(012) = 0$.

Now equations (4) and (6) give $\boldsymbol{D}(011) = \boldsymbol{D}(01\bar{1})$ and $\boldsymbol{D}(012) = \boldsymbol{D}(01\bar{2})$, and hence $\boldsymbol{D}(011) = \boldsymbol{D}(012) = \mathbf{0}$. Combining with (6), we finally get

$$\boldsymbol{d}_1 = \boldsymbol{d}_3 = \boldsymbol{d}_5 = \boldsymbol{d}_7 = \boldsymbol{d}_9 = \boldsymbol{d}_{11} = \boldsymbol{d}_{13} = \boldsymbol{d}_{15} = \mathbf{0}. \tag{7}$$

Thus the cell doubling in the magnetic structure is due to the moments in the (octahedral) sites 17–24 only. These are called B(d) in the following, as opposed to B(nd) for the 'non-doubling' B sites 9–16.

4.1.2. k even. The arguments are similar to those already shown. Based on (4) and the pairs of zero-intensity reflections $\{(220), (\bar{2}20)\}$, $\{(140), (\bar{1}40)\}$ and $\{(22\bar{2}), (26\bar{2})\}$, the following result is obtained:

$$\boldsymbol{p}_1 - \boldsymbol{p}_5 = \boldsymbol{p}_3 - \boldsymbol{p}_7 = \boldsymbol{p}_9 - \boldsymbol{p}_{13} = \boldsymbol{p}_{11} - \boldsymbol{p}_{15} = \boldsymbol{p}_{17} - \boldsymbol{p}_{21} = \boldsymbol{p}_{19} - \boldsymbol{p}_{23} = \mathbf{0}. \tag{8}$$

Until now, a common (isotropic) form factor for all ions has been assumed. However, (6), (7) and (8) can be derived even if two different form factors, one common to all A sites and the other common to all B sites, are assumed. This will be of interest later.

For the 10 zero-intensity reflections not used so far (see top of table 2), the calculated intensity is zero because of (6), (7) and (8). Thus, these relations contain all the information obtainable from reflections with $I = 0$, and they lead to the following general rules for the magnetic intensities for Mn_3O_4 (at 4·7 K), valid for the nuclear intensities also:

$$(a) \text{ for } k \text{ odd}, \qquad I = 0 \qquad \text{if } h \text{ is even} \tag{9a}$$

$$(b) \text{ for } k \text{ even}, \qquad I = 0 \qquad \text{if } h + \frac{k}{2} + l \text{ is odd} \tag{9b}$$

Equations (7) and (8) give for the moments $\boldsymbol{\mu}_1$ to $\boldsymbol{\mu}_{16}$ the relations below, where in addition 6 new vectors $\boldsymbol{T}_1$ to $\mathbf{0}_4$ are defined:

$$\left.\begin{aligned} &\boldsymbol{\mu}_1 = \boldsymbol{\mu}_2 = \boldsymbol{\mu}_5 = \boldsymbol{\mu}_6 \qquad && \boldsymbol{T}_1 \equiv \boldsymbol{\mu}_1 + \boldsymbol{\mu}_2 + \boldsymbol{\mu}_5 + \boldsymbol{\mu}_6 = 4\boldsymbol{\mu}_1 \\ &\boldsymbol{\mu}_3 = \boldsymbol{\mu}_4 = \boldsymbol{\mu}_7 = \boldsymbol{\mu}_8 && \boldsymbol{T}_2 \equiv \boldsymbol{\mu}_3 + \boldsymbol{\mu}_4 + \boldsymbol{\mu}_7 + \boldsymbol{\mu}_8 = 4\boldsymbol{\mu}_3 \\ &\boldsymbol{\mu}_9 = \boldsymbol{\mu}_{10} = \boldsymbol{\mu}_{13} = \boldsymbol{\mu}_{14} && \mathbf{0}_1 \equiv \boldsymbol{\mu}_9 + \boldsymbol{\mu}_{10} + \boldsymbol{\mu}_{13} + \boldsymbol{\mu}_{14} = 4\boldsymbol{\mu}_9 \\ &\boldsymbol{\mu}_{11} = \boldsymbol{\mu}_{12} = \boldsymbol{\mu}_{15} = \boldsymbol{\mu}_{16} && \mathbf{0}_2 \equiv \boldsymbol{\mu}_{11} + \boldsymbol{\mu}_{12} + \boldsymbol{\mu}_{15} + \boldsymbol{\mu}_{16} = 4\boldsymbol{\mu}_{11} \end{aligned}\right\} \tag{10a}$$

$$\left.\begin{aligned} &\mathbf{0}_3 \equiv \boldsymbol{\mu}_{17} + \boldsymbol{\mu}_{18} + \boldsymbol{\mu}_{21} + \boldsymbol{\mu}_{22} \\ &\mathbf{0}_4 \equiv \boldsymbol{\mu}_{19} + \boldsymbol{\mu}_{20} + \boldsymbol{\mu}_{23} + \boldsymbol{\mu}_{24}. \end{aligned}\right\} \tag{10b}$$

For these vectors we introduce the following assumptions:

$$|\boldsymbol{T}_1| = |\boldsymbol{T}_2|, |\mathbf{0}_1| = |\mathbf{0}_2| \text{ and } |\boldsymbol{\mu}_i| = |\boldsymbol{\mu}_k|, i, k \geqslant 17, \tag{11}$$

ie: the moments are assumed of equal magnitude within each of the 3 groups of sites A, B(nd) and B(d). Essentially, equation (11) contain the first and, as will appear later, the only assumptions made in the present magnetic structure determination.

The relations among the B(d) moments are slightly more complicated than (10*a*). It can be shown from (6), (8) and (11) that only two possibilities exist:

(i) $\boldsymbol{d}_{17} = \pm \boldsymbol{d}_{19}$ and $|\mathbf{0}_3| = |\mathbf{0}_4|$, but not necessarily $\mathbf{0}_3 = \mathbf{0}_4$.
(ii) $\mathbf{0}_3 = \mathbf{0}_4$ and $|\boldsymbol{d}_{17}| = |\boldsymbol{d}_{19}|$, but not necessarily $\boldsymbol{d}_{17} = \pm \boldsymbol{d}_{19}$.

Furthermore, $\mathbf{0}_3$ and $\mathbf{0}_4$ must in both cases be perpendicular to the plane or line defined by $\boldsymbol{d}_{17}$ and $\boldsymbol{d}_{19}$. (It will appear later that the final structure satisfies both (i) and (ii)).

4.2. Non-zero intensity reflections

4.2.1. k odd. (18 reflections were measured). According to (7), only the B(d) sites, and hence only Mn^{3+} ions, contribute to these reflections. Assuming a common form factor for these sites, the intensity can be written, using (3), (6) and (7):

$$I(hkl) = (\tfrac{1}{2}r_0\gamma f)^2[4|\boldsymbol{d}_{17}|^2 \sin^2 V_{17} + 4|\boldsymbol{d}_{19}|^2 \sin^2 V_{19}]/\cos\theta, \tag{12}$$

where V_{17} is the angle between $\boldsymbol{d}_{17}$ and $\boldsymbol{H}$, and V_{19} is defined similarly. The expression in [ ] is $|\boldsymbol{Q}|^2$, see equation (4). Information on the form factor can, without knowledge of $\boldsymbol{d}_{17}$ and $\boldsymbol{d}_{19}$, be obtained from (12), because $|\boldsymbol{Q}|^2$ is the same for reflections having the same direction of $\boldsymbol{H}$. Applied to our data, the ratios $f(110)/f(330)$, $f(\bar{1}10)/f(\bar{3}30)$ and $f(11\bar{1})/f(33\bar{3})$ can thus be found in a 'structure independent' way. A comparison (figure 2) with the form factor for Mn^{2+} (Hastings *et al* 1969) shows, that $f_{Mn^{2+}}$ is not applicable to Mn^{3+}. Instead, we have adopted a form factor given by the following (based on the criterion of obtaining a satisfactory fit to the experimental points in figure 2)

$$f_{Mn^{3+}}\left(\frac{\sin\theta}{\lambda}\right) = f_{Mn^{2+}}\left(\frac{0{\cdot}9\sin\theta}{\lambda}\right), \tag{13}$$

where $f_{Mn^{2+}}$ is taken from Hastings *et al* (1959).

The values of $|\boldsymbol{Q}|$, derived from the observed I's through (12), are found to have a simple relation to the direction of $\boldsymbol{H}$: apart from experimental errors, $|\boldsymbol{Q}(hkl)|$ is proportional to $\cos u$, where u is the angle between $\boldsymbol{H}$ and the plane (001). This points to a model where $\boldsymbol{d}_{17}$ and $\boldsymbol{d}_{19}$ are both perpendicular to the (001) plane. A least squares analysis confirmed this and gave the length $|\boldsymbol{d}_{17}| = |\boldsymbol{d}_{19}| = 6{\cdot}14 \pm 0{\cdot}10$ in units of μ_B. The R value is 5·1 % (based on F's) for the 18 reflections. It follows (see end of §4.1) that $\mathbf{0}_3$ and $\mathbf{0}_4$ are both perpendicular to the [001] direction. The two alternatives (*a*): $\boldsymbol{d}_{17} = \boldsymbol{d}_{19}$ and (*b*): $\boldsymbol{d}_{17} = -\boldsymbol{d}_{19}$ still possible are only apparently different. Actually, a translation $(\frac{1}{2}, \frac{1}{4}, \frac{1}{2})$ brings the pattern based on (*a*) in coincidence with that for (*b*).

In order to prove the uniqueness of the configuration found, the 18 equations of the form (12) were solved for the unknown quantities $\boldsymbol{d}_{17}$ and $\boldsymbol{d}_{19}$ with the constraint $|\boldsymbol{d}_{17}| = |\boldsymbol{d}_{19}|$. A graphical method, useful for this overdetermined set of equations, gave the result that only two solutions exist: the one given above, and a configuration where (approximately) $\boldsymbol{d}_{17} = (2{\cdot}3, -6{\cdot}8, 3{\cdot}5)$ and $\boldsymbol{d}_{19} = (-6{\cdot}8, -2{\cdot}3, 3{\cdot}5)$ in units of μ_B. The latter can however be excluded, because it requires $\mathbf{0}_3 = \mathbf{0}_4$ to have a direction (see end of §4.1), which makes it impossible to obtain a fit to the data for k even. This was proved by a method similar to the one mentioned below.

4.2.2. k even. (35 reflections measured). The form factor given by Hastings *et al* was used for all A sites, the one given in (13) for all B sites. In establishing the main features of the structure, the average $\langle f \rangle$ of the two form factors can be used with sufficient accuracy. The magnetic intensity can then be written

$$I = (\tfrac{1}{2}r_0\gamma\langle f\rangle)^2[|\boldsymbol{P}_r|^2 \sin^2 V_r + |\boldsymbol{P}_i|^2 \sin^2 V_i]/\cos\theta, \tag{14}$$

where $\boldsymbol{P}_r$ and $\boldsymbol{P}_i$ are, respectively, the real and the imaginary part of $\boldsymbol{P}$, equation (4), and V_x(x = r or i) is the angle between $\boldsymbol{P}_x$ and $\boldsymbol{H}$. The values of $|\boldsymbol{Q}|$ (the square root of the expression in [ ] in (14)) as found from experiment is given in table 2.

Calculation of $\boldsymbol{P}_r$ and $\boldsymbol{P}_i$ for an arbitrary reflection (hkl) with both k and $h + k/2 + l$

even leads to a result contained in the following general expressions:

$$\boldsymbol{P}_r = c_1(\boldsymbol{T}_1 + \boldsymbol{T}_2) \pm (\boldsymbol{0}_1 \pm \boldsymbol{0}_2) \pm (\boldsymbol{0}_3 \pm \boldsymbol{0}_4) \tag{15a}$$

$$\boldsymbol{P}_i = c_2(\boldsymbol{T}_1 - \boldsymbol{T}_2) \tag{15b}$$

where $(c_1, c_2) = (1, 0), (0,1)$ or $(\sqrt{2}/2, \sqrt{2}/2)$.

Furthermore, for $c_1 = 1$ or 0 the signs in front of $\mathbf{0}_2$ and $\mathbf{0}_4$ are the same, whereas for $c_1 = \sqrt{2}/2$ these signs are opposite. Thus, only 20 different types of $\boldsymbol{P}$ can occur. (To obtain (15), $\boldsymbol{P}$ must be multiplied by a physically irrelevant phase factor for certain reflections, and in other cases the complex conjugate $\boldsymbol{P}^*$ is given instead of $\boldsymbol{P}$).

Relations so far found (or assumed) among the vectors in (15) can be summarized thus:

$$|\boldsymbol{T}_1| = |\boldsymbol{T}_2| \qquad |\boldsymbol{0}_1| = |\boldsymbol{0}_2| \qquad |\boldsymbol{0}_3| = |\boldsymbol{0}_4|,$$

and both $\mathbf{0}_3$ and $\mathbf{0}_4$ are perpendicular to [001]. Finally, from magnetization measurements (Dwight and Menyuk 1960, Nielsen 1971) we get the relation

$$\boldsymbol{M} \equiv \boldsymbol{T}_1 + \boldsymbol{T}_2 + \boldsymbol{0}_1 + \boldsymbol{0}_2 + \boldsymbol{0}_3 + \boldsymbol{0}_4 = (0, 15{\cdot}1, 0)\mu_B.$$

From the preceding information, the magnetic structure can be found by a method to be described briefly: For the reflection (040) we have $\boldsymbol{P}_i = \mathbf{0}$ and $\boldsymbol{P}_r = \boldsymbol{M} - 2(\boldsymbol{0}_1 + \boldsymbol{0}_2)$. The weak intensity shows that $\mathbf{0}_1 + \mathbf{0}_2$ is nearly parallel to the b axis. Now, from several medium-intensity reflections as eg (± 120) and (± 320) where $c_2 = 1$ (equation (15)), it can be concluded that $|\boldsymbol{T}_1 - \boldsymbol{T}_2|$ is small in the sense that the main contribution to the strongest reflections is due to $\boldsymbol{P}_r$. This makes possible a graphical method using the 7 reflections of largest $|\boldsymbol{Q}|$ value in addition to $(\bar{1}22)$. It leads to the following (approximate) relations as the only possibility, taking into consideration any length and direction for the vectors $\boldsymbol{T}_1 + \boldsymbol{T}_2, \mathbf{0}_1, \mathbf{0}_2, \mathbf{0}_3$ and $\mathbf{0}_4$ compatible with the relations summarized above:

$$\boldsymbol{T}_1 + \boldsymbol{T}_2 \simeq (0, 30, 0) \qquad \boldsymbol{0}_3 \simeq \boldsymbol{0}_4 \simeq (0, -4, 0) \qquad \boldsymbol{0}_1 - \boldsymbol{0}_2 \simeq (0, 0, -30)$$
$$\text{and } \boldsymbol{0}_1 + \boldsymbol{0}_2 \simeq (0, -8, 0) \text{ in units of } \mu_B. \tag{16}$$

In particular, we found no indication that $\boldsymbol{T}_1 + \boldsymbol{T}_2$ deviates from the $\boldsymbol{b}$ direction. Based on this, the least squares refinement was performed with the constraint that $\boldsymbol{T}_1 + \boldsymbol{T}_2, \mathbf{0}_1 + \mathbf{0}_2$ and $\mathbf{0}_3 + \mathbf{0}_4$ were all of the form $(0, y_i, 0)$ with $y_1 + y_2 + y_3 = 15{\cdot}1$, giving a total of 7 free parameters. Included in the refinement were only those reflections (17 in all), where the magnetic intensity exceeds the nuclear. The parameters found are given in table 3. The R value is 3·3 % (based on F's) for the 17 reflections mentioned. For the remaining 18 nonzero intensities, there are in some cases large deviations between calculated and observed F values, if the latter are based on the magnetic intensity as given by $I_{exp}(4\,K) - I_{exp}(300\,K)$ (see table 2, columns 4 and 5). These deviations are however largely due to the change in extinction mentioned in § 3. This is seen when $I_{exp}(4\,K)$ is compared with the calculated total intensity at 4 K, the nuclear intensity now being derived from the nuclear parameters instead of being taken from the 300 K data. Columns 8 and 9 in table 2 give the corresponding 'total F values', showing that only the 4 strongest reflections have appreciable extinction at 4 K. The R value for the remaining 70 reflections is 4·7 % (based on F's) or 9·2 % (based on intensities).

The configuration found is shown in figure 3. The magnetic space group is $P2_1/b$ in the notation used by Opechowski and Guccione (1965). A comparison with the structure published by Boucher *et al* will be given in § 6.

Table 3. Mn_3O_4. Ion moment magnitudes μ in Bohr magnetons and direction cosines $(\alpha_1, \alpha_2, \alpha_3)$ referred to $(\boldsymbol{a}, \boldsymbol{b}, \boldsymbol{c})$ $(|\boldsymbol{b}| = 2|\boldsymbol{a}|)$. For numbering: see figure 3.

			4·7 K		
Type of site	Ion no.	μ	α_1	α_2	α_3
A	1, 2, 3, 4, 5, 6, 7, 8	4·34 ± 10	0·00 ± 0·15	1·00	0·00 ± 0·15
B(nd)	9, 10, 13, 14,	3·64 ± 8	−0·09 ± 0·05	−0·38 ± 0·02	−0·92 ± 0·01
	11, 12, 15, 16,	3·64 ± 8	0·09 ± 0·05	−0·38 ± 0·02	0·92 ± 0·01
B(d)	17, 20, 21, 24,	3·25 ± 6	0·00 ± 0·06	−0·33 ± 0·02	−0·94 ± 0·01
	18, 19, 22, 23	3·25 ± 6	0·00 ± 0·06	−0·33 ± 0·02	0·94 ± 0·01
			29 K		
Type of site	Ion no.	μ	α_1	α_2	α_3
A	1, 2, 3, 4, 5, 6, 7, 8	3·78 ± 12	0·00 ± 0·12	1·00	0·00 ± 0·12
B(nd)	9, 10, 13, 14,	3·05 ± 8	−0·12 ± 0·07	−0·40 ± 0·03	−0·91 ± 0·01
	11, 12, 15, 16,	3·05 ± 8	0·12 ± 0·07	−0·40 ± 0·03	0·91 ± 0·01
B(d)	17, 20, 21, 24,	3·17 ± 8	0·00 ± 0·04	−0·25 ± 0·03	−0·97 ± 0·01
	18, 19, 22, 23	3·17 ± 8	0·00 ± 0·04	−0·25 ± 0·03	0·97 ± 0·01

5. Evolution of the structure with temperature

Heating the sample from 4·7 K we find the intensity $I(110)$ very constant up to 32·8 K, at which temperature a phase transition occurs (see below). At 29 K (ie below the transition) we have repeated our intensity measurements on all (h, k_{even}, l) reflections. A numerical analysis, in which the model at 4·7 K was retained, gave the ion moments as listed in table 3.

At the transition point (32·8 K) we observe a drop in $I(110)$ to about half its low temperature value. Further heating reveals a position shift τ of the reciprocal lattice point corresponding to neutron scattering. We find the shift directed along the positive $\boldsymbol{b}^*$, ie the shifted 'reciprocal lattice point' has the coordinates $(1, 1 + \tau, 0)$ where $\tau > 0$. In fact we find all (h, k_{odd}, l) reflections shifted parallel to the $\boldsymbol{b}^*$ axis according to the following rules:

$$\text{if } \left(\frac{k+1}{2} + l\right) \text{ is odd: } (h, k_{\text{odd}} + \tau, l) \tag{17a}$$

$$\text{if } \left(\frac{k+1}{2} + l\right) \text{ is even: } (h, k_{\text{odd}} - \tau, l). \tag{17b}$$

Other intensities such as $I(120)$ (see figure 4) and the powder reflections $I(120)$, $I(101)$ and $I(122)$ measured by Boucher *et al* (1971) showed no discontinuity at 32·8 K, from which we conclude that the phase transition only occurs in the cell doubling spin system. We have furthermore experimentally ascertained that no additional reflections occur in the ranges $(h, k \pm \tau, l)$, k odd and even.

The shifts may be explained in terms of a modulation of the cell doubling moments. However, because the saturation magnetization shows no discontinuity at the transition point (Dwight and Menyuk 1960, Nielsen 1971) we conclude that only the x and z components participate in the modulation (x axis$||\boldsymbol{a}$, y axis$||\boldsymbol{b}$, z axis$||\boldsymbol{c}$). The x and z

components of the individual moments may be written in the following form:

$$\mu^n_{jx} = \mu'_x \cos 2\pi(qn + \phi_{jx}) \qquad j = 17, \ldots 24 \tag{18a}$$

$$\mu^n_{jz} = \mu'_z \cos 2\pi(qn + \phi_{jz}) \qquad j = 17, \ldots 24. \tag{18b}$$

$q = |\boldsymbol{q}|$, where $\boldsymbol{q}$ is the propagation vector in units of $\boldsymbol{b}^*$ ($q = 1 - \tau$) and n is the cell labelling along the y axis (the cell is still chosen as a doubled chemical BC unit cell).

The q dependence of the phases ϕ in (18) is partly determined by the 'selection rules' (17). We find $\phi_{jx} = \phi_{jz} + \alpha$, where α is a phase constant which cannot be determined from (17) alone.

Assuming (as for the 4 K structure) a constant magnitude of the ion moments, we must have $\mu'_x = \mu'_z = \mu'$ and $\alpha = \pm\frac{1}{4}$. In this case (18) represents a conical structure with [010] as cone axis. For μ^n_{jz} we find (apart from an arbitrary common phase):

$$\mu^n_{17z} = -\mu^n_{23z} = -\mu' \cos 2\pi qn;\ \mu^n_{19z} = -\mu^n_{21z} = \mu' \cos 2\pi q(n + \tfrac{1}{4}) \tag{19a}$$

$$\mu^n_{18z} = -\mu^n_{24z} = -\mu' \cos 2\pi q(n + \tfrac{1}{2});\ \mu^n_{20z} = -\mu^n_{22z} = \mu' \cos 2\pi q(n + \tfrac{3}{4}). \tag{19b}$$

For the x components, read sin instead of cos.

It must be emphasized that equation (19) with $q = 1$ *does not* represent the low temperature configuration; instead, $q = 1$ represents another configuration, which however has the same unit cell as found at 4 K.

Assuming equal ion moment magnitudes, we may compare the neutron scattering intensities for the two structures. Defining $I^{LT}_{(110)}$ as the intensity of the (110) reflection at low temperature, and $I^{q=1}_{(110)}$ as the equivalent intensity calculated from configuration (19) ($q = 1$), we find $I^{q=1}_{(110)}/I^{LT}_{(110)} = \frac{3}{5}$. Figure 4 shows that the measured intensities are in accordance with this expression.

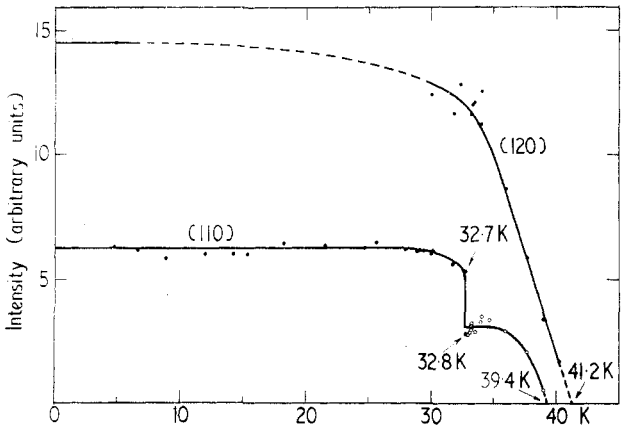

Figure 4. Neutron intensities for (120) and (110) reflections, which are of pure magnetic origin (see table 2). ●Correspond to 'unshifted' reciprocal lattice points; ○Correspond to 'shifted' reciprocal lattice points. Notice the low intensity point ● at $T = 32{\cdot}8$ K.

With increasing temperature q decreases, as shown in figure 5, until 39·4 K where the corresponding intensities become zero.

Between 39·4 K and 41 K we conclude that the magnetic cell is coincident with the chemical BC unit cell.

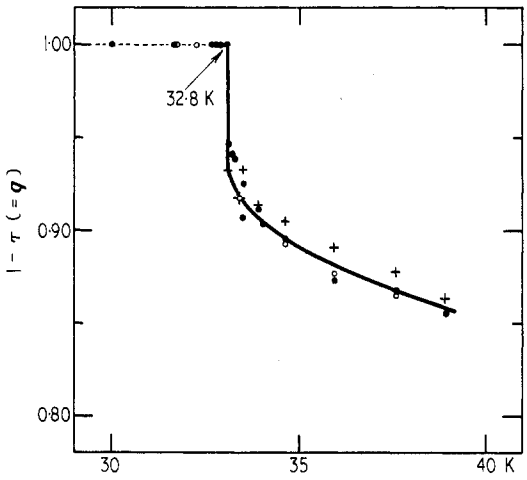

Figure 5. Measured values of the propagation vector magnitude q against temperature. The values $q = 1$ ($\tau = 0$) for $T < 32{\cdot}8$ K correspond to the low temperature structure. The phase transition occurs at $T = 32{\cdot}8$ K where $q = 1{\cdot}0$. Immediately above $T = 32{\cdot}8$ K, q shows an abrupt change with temperature. ● (110); ○ '($\frac{1}{2}$20)'; + (130).

6. Discussion

As mentioned above, the magnetic structure proposed in the present work deviates somewhat from the structure previously reported by Boucher *et al* (1971), referred to as BBP below. The difference can qualitatively be described as follows. (1) In our model, all tetrahedral moments are aligned ferromagnetically in the $\boldsymbol{b}$ direction, whereas in the model of BBP these moments alternately have a component in the $\boldsymbol{c}$ and $-\boldsymbol{c}$ direction ($T_{1z} = -T_{2z} \neq 0$). It is noted, however, that in our case the x and z components of the tetrahedral moments have comparatively large inaccuracies (see table 3). The reason for this is obvious from equation (15): Nonzero T_x and T_z values would give rise to a nonzero, but small value of $|\boldsymbol{T}_1 - \boldsymbol{T}_2|$ (our data show definitely that T_x and T_z are small compared to T_y). Now, because $\boldsymbol{T}_1 - \boldsymbol{T}_2$ is not combined linearly with other vectors in calculating the intensity, its contribution will for almost any reflection be dominated by the contributions from either P_r or the nuclear scattering. Thus, it is doubtful whether a much more accurate determination of $\boldsymbol{T}_1 - \boldsymbol{T}_2$ is possible at all. The lengths of the tetrahedral moments also differ somewhat: 4·65 μ_B (BBP) and 4·34 μ_B (present work). The value found by us is indeed very low for an S state ion. For the free ion Mn^{2+} the lowest excited state is 3·3 eV above the ground state, and hence one would expect a value close to 5 μ_B. However, in view of the care exercised in the determination of the scale factor (§ 3), we consider our value reliable. (2) In the model of BBP, all octahedral moments have a common length of 3·55 μ_B. Our data give here a clear indication of different lengths for the moments in sites B(nd) and B(d). For the B(nd) moments, BBP give the x component as zero, where we find a value which, although small, is significantly different from zero. On the other hand, for the B(d) moments BBP have a nonzero component, where in our case this component does not differ significantly from zero.

For comparison of the two models, we have calculated the R factor for the 17

magnetically strong reflections used in the refinement mentioned in §4.2. For the model of BBP the R value is 11% as opposed to 3·3% obtained above.

Concerning the model proposed by us, the following can be mentioned.

In order to visualize the difference in crystallographic surroundings for octahedral site Mn ions which do and do not contribute to the magnetic cell doubling respectively, we may divide the Mn-occupied oxygen octahedrons in two classes. The octahedrons (equal in shape) are distorted in such a way that only C_{2h} symmetry remains. Half of them (say class 1) are situated with their mirror planes parallel to the chemical (100) plane, whereas the other half (class 2) have their mirror planes parallel to the chemical (010) plane (see figure 6). Two adjacent octahedrons in the same class (for example no. 10 and 11) are symmetry related through a mirror operation.

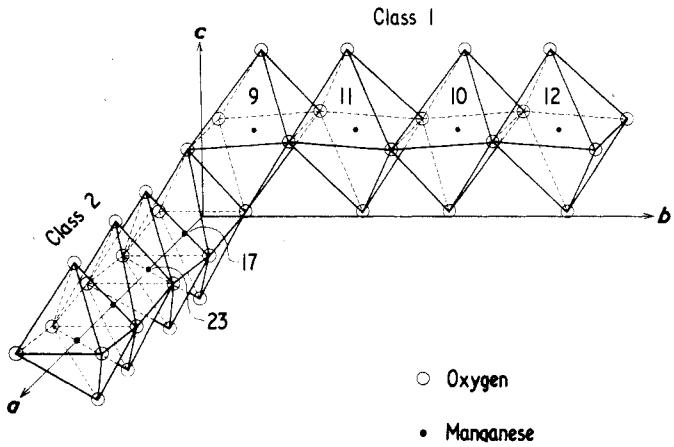

Figure 6. Oxygen surroundings for B(nd) sites (Class 1) and B(d) sites (Class 2). The Mn ions in sites B(nd) do not contribute to the cell doubling contrary to those in sites B(d). (The magnetization is in the b direction). ○ oxygen; ● manganese.

The non doubling Mn ions in B(nd) sites (constituting $\mathbf{0}_1 + \mathbf{0}_2$) occupy one of the classes, class 1 in figure 6, and the doubling Mn ions in B(d) sites (constituting $\mathbf{0}_3 + \mathbf{0}_4$) occupy class 2.

From the values of ion moments in B(nd) sites listed in table 3 it is evident that all these moment directions are equal with respect to oxygen surroundings, ie the moments are symmetry related through the same mirror operations as are the octahedrons. This means that even an anisotropic g factor for Mn^{3+} ions in these surroundings will result in the same magnetic moment magnitude for all these sites. A similar result is found for ions in B(d) sites, but an obvious difference exists between the two classes as regards moment directions with respect to oxygen surroundings. This may explain the different moment magnitudes found for ions in B(nd) and B(d) sites respectively.

For the present structure it is easily shown from simple symmetry arguments that the crystal anisotropy energy $\mathscr{F}_A$ has an extremum for $\boldsymbol{M}$ pointing along the b axis. This proves the b axis as the easy direction of magnetization. In the BBP structure, on the contrary, we find because the B(d) site moments have non zero x components, that an extremum in $\mathscr{F}_A$ may occur only accidentally for $\boldsymbol{M}$ pointing along the b axis. Although a very accurate measurement of the magnetization direction in zero applied field *may* show a deviation from $\boldsymbol{b}$, we conclude from the measurements by Dwight and Menyuk (1960) and Nielsen (1971) that this deviation is very small.

It should also be noted that the present low-temperature structure for Mn_3O_4 is included among the 24 degenerate configurations proposed by Dwight and Menyuk (1960) on the basis of a generalized Yafet–Kittel model. In fact Dwight and Menyuk's analysis yielded our equation (6) and (7) and most of equation (8) ($\boldsymbol{p}_1 - \boldsymbol{p}_5 = \boldsymbol{p}_3 - \boldsymbol{p}_7 = \boldsymbol{0}$; $\boldsymbol{p}_9 - \boldsymbol{p}_{13} - (\boldsymbol{p}_{15} - \boldsymbol{p}_{11}) = \boldsymbol{p}_{17} - \boldsymbol{p}_{21} - (\boldsymbol{p}_{19} - \boldsymbol{p}_{23}) = \boldsymbol{0}$).

Acknowledgments

We are greatly indebted to Dr B Lebech, not only for the permission for us to use the neutron spectrometer, but also for many stimulating discussions and suggestions. The helpful assistance from the staff of Physics Department at the Danish Atomic Energy Commission Research Establishment Risö is also gratefully acknowledged. Finally, we would like to thank Professor V Frank for many helpful discussions and Professor A Nielsen for his continued interest.

References

Boucher B, Buhl R and Perrin M 1971 *J. Phys. Chem. Solids* **32** 2429–37
Dwight K and Menyuk N 1960 *Phys. Rev.* **119** 1470–9
Goodenough J B and Loeb A L 1955 *Phys. Rev.* **98** 391–408
Hastings J M, Elliott N and Corliss L M 1959 *Phys. Rev.* **115** 13–7
Kasper J S 1959 *Bull. Am. Phys. Soc.* **4** 178
Moruzzi V L 1961 *J. appl. Phys.* **32** suppl. 59–61
Nielsen O V 1969 *J. Cryst. Growth* **5** 398–400
Nielsen O V 1971 *J. Phys., Paris* **32** suppl. 51–2
Opechowski W and Guccione R 1965 *Magnetism* Vol IIA ed G T Rado and H Suhl (New York: Academic Press) pp 105–65
Satomi K 1961 *J. Phys. Soc. Japan* **16** 258–66